Delft University of Technology

Evaluation of photocatalytic micro-surfacing mixture
road performance, vehicle exhaust gas degradation capacity and environmental impacts

Zhang, Zhao; Liu, Kai; Chong, Dan; Niu, Dongyu; Lin, Peng; Liu, Xueyan; Niu, Yanhui; Jing, Ruxin

Evaluation of photocatalytic micro-surfacing mixture: road performance, vehicle exhaust gas degradation capacity and environmental impacts

Zhao Zhang [a,b], Kai Liu [a,b], Dan Chong [c], Dongyu Niu [a,b,d,*], Peng Lin [d,*], Xueyan Liu [d], Yanhui Niu [a,b], Ruxin Jing [d]

[a] Engineering Research Center of Transportation Materials of the Ministry of Education, Chang'an University, Xi'an 710061, China
[b] School of Materials Science and Engineering, Chang'an University, Xi'an 710061, China
[c] Department of Management Science and Engineering, Shanghai University, Shanghai 20044, China
[d] Faculty of Civil Engineering & Geosciences Delft University of Technology Stevinweg 1, 2628 CN Delft, The Netherlands

ARTICLE INFO

ABSTRACT

To purify severe air pollution in traffic-intensive urban areas and tunnels, an innovative type of photocatalytic micro-surfacing mixture (PMM) was designed, which was enhanced by polypropylene (PP) fiber and nano-TiO₂. In this work, the road performance of sixteen PMMs with the different contents of PP and nano-TiO₂ were evaluated by wet-track abrasion test, wheel rutting deformation test and low-temperature splitting test. The vehicle exhaust (VE) gas degradation capacity of sixteen PMMs was characterized under ultraviolet (UV) light and visible light conditions. The life cycle assessment (LCA) methodology was applied to evaluate the environmental impact of PMM. The results showed that the road performances of PMM were improved with the increase of the PP fibers amount. The VE gas degradation capacity was significantly enhanced with the increase of nano-TiO₂ amount. PMM with 0.2 wt% PP fibers and 60 wt% replacement of mineral filler with nano-TiO₂ was a viable alternative to improve photocatalytic degradation of VE in pavement engineering. In addition, the modified micro-surfacing mixture facilitates a significant reduction in energy consumption and greenhouse gas emissions.

1. Introduction

With the rapid development of the Chinese economy, the number of vehicles has grown at an alarming rate [1]. The annual sales of on-road vehicles have grown from roughly 13.64 million in 2009 to 28 million in 2016, as shown in Fig. 1 [2]. Furthermore, the vehicle exhausts (VE) is emitted due to incomplete combustion of hydrocarbon fuel in internal combustion engines, including carbon monoxide (CO), nitrogen oxides (NOx), hydrocarbon compound (HC), and other components [3–4]. According to the statistical data of the Chinese government, the emissions of CO, HC, NOx has remained at a high level in recent years, as shown in Fig. 2 [5]. These exhaust gases will seriously damage human health, such as cardiovascular disease and cancer [6–8]. More than that, the increasing number of studies suggests VE has been identified as one of the most important contributors to air pollution in most cities in China [9–12]. Meanwhile, VE in traffic-intensive urban areas and tunnels can be extremely harmful to human beings [13–17]. Therefore, VE degradation has become an important and urgent problem now.

At present, photocatalytic materials are used to degrade VE into pavement surfaces [18]. Owing to the strong photocatalytic degradation ability, the chemical and thermal stability, and nontoxicity of TiO₂ [19,20], it is mainly adopted as a photocatalytic material in the pavement to purify VE. For example, in 1999, TiO₂ was first used in cement pavement and exhibited good photocatalytic performance for purifying NOₓ in Japan [21]. Tan et al. [22] presented the dosage percentage of TiO₂ is from 50% to 60% of mineral powder in asphalt mixture. It degraded VE with good effect, but the performance of asphalt mixture had a little negative effect. Boonen and Beeldens [23], investigated the effect of photocatalytic materials on exhibiting air-purifying properties in concrete pavement. In addition, the photocatalytic concrete materials by adding TiO₂ were introduced from lab tests to field scale applications. However, uniform testing methods are lacking in evaluating photocatalytic activity in Europe. Xia et al. [24,25] studied TiO₂ Waterborne Coating as photocatalytic oxidation to degrade pollutants under visible light and ultraviolet (UV) light. The photocatalytic coating exhibited favorable reusability and durability and can be applied to new or old

---
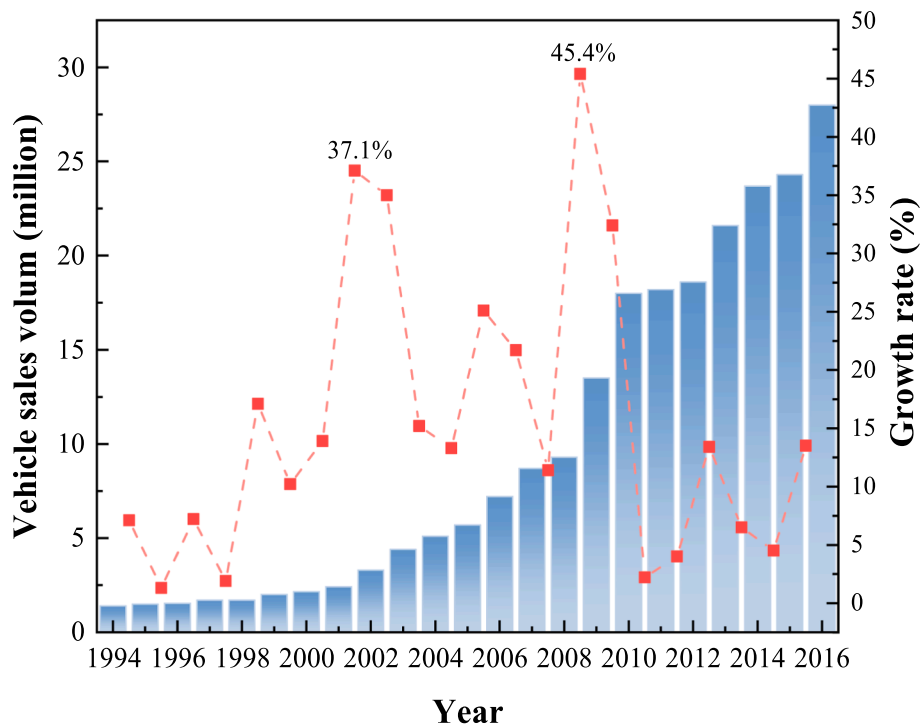
Fig. 1. Vehicle sales volume and growth rate in China from 1994 to 2016 [2].
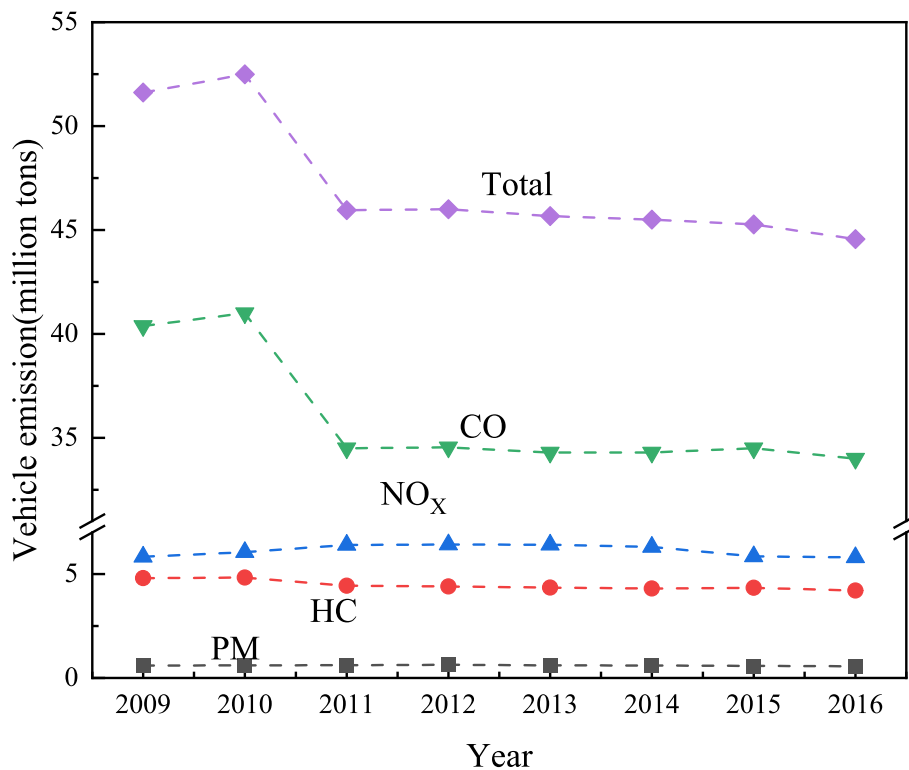
Fig. 2. The amount of air pollutants from the vehicle in China from 2009 to 2016 (data from China MEP, 2010–2016) [5].

sections of the road. In short, TiO_2 is widely used as a photocatalytic additive in pavement materials and has an excellent VE Degradation effect. However, some limitations are presented, such as the negative effect of pavement performance and the lack of uniform purifying performances testing methods.

On the other hand, micro-surfacing mixture is one of the most

important pavement materials as an economical, rapid, and effective preventive maintenance material, which is composed of aggregate, filler, polymer modified emulsified asphalt binder, additives and water. The skid-resistance, moisture damage resistance and anti-aging properties of pavement are improved with the application of micro-surfacing mixture. The thickness of micro-surfacing mixture layer is normally

Table 1
Technical indexes of SBR modified emulsified asphalt binder.

Test	Value	Specification	Test method
Penetration (25 ℃, 100 g, 5 s)/0.1 mm	68	40 ~ 90	ASTM D5, 2013
Ductility (5 ℃)/cm	65	≥20	ASTM D113, 2007
Softening point (℃)	59.3	≥57	ASTM D36, 2014
Evaporation residue content (%)	65.2	≥62	ASTM D6997, 2004
Residual on sieve (1.18 mm)/%	0.02	≤0.1	ASTM D244, 2017
Storage stability (1d)/%	0.03	≤ 1	ASTM D6997, 2004
Viscosity (25℃)/s	19	16 ~ 20	JTG E20 T0621-1993

Table 2
Nano-TiO$_2$ technical indicators.

Test projects	Test results	Standard requirements
TiO$_2$ content (%)	≥99	98 ~ 99.5
Grain size (nm)	10 ~ 20	≤20
Specific surface area (m^2/g)	80 ~ 220	80 ~ 110
Packing density (g/cm^3)	0.24	≤0.5
pH	6.0 ~ 6.5	6.0 ~ 6.5
Scorch weight reduction (%)	≤1.0	≤3.5

Table 3
Technical specifications of PP fibers.

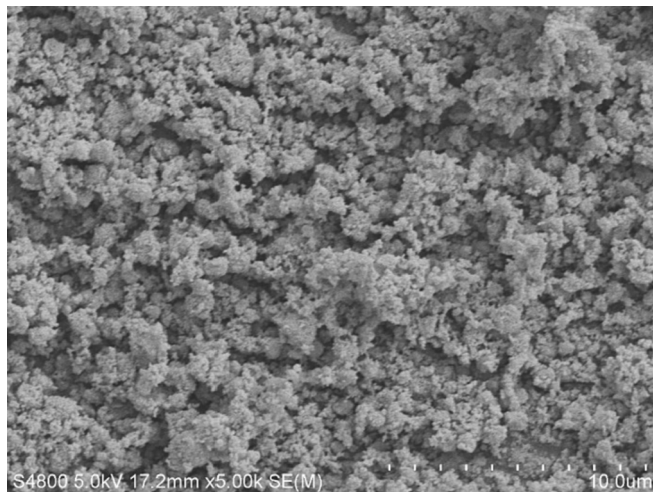| Index	Test results	Standard requirements
Equivalent diameter (mm)	0.028	0.015 ~ 0.035
Density (g/cm^3)	0.920	0.910 ± 0.040
Length (mm)	16	10 ~ 38
Tensile strength (MPa)	496	≥270
Elongation at break (%)	21	≥8.0
Melting point (℃)	185	≥160

Fig. 3. The SEM image of nano-TiO$_2$.

from 4 mm to 8 mm as a sealing layer of pavement structure [26,27]. It is considered as an ideal matrix for photocatalytic additives. As the thickness is less than 8 mm, it ensures that the photocatalytic additives can be effectively exposed to visible light and UV light to degrade VE. Meanwhile, it has a certain thickness to ensure that the photocatalytic particles will not peel off due to the abrasion of the pavement surface by vehicles. For example, Xu et al. [28] proposed the rubber-titanium-aluminum ultrafine-grained micro-surfacing mixture for VE degradation. Thus, micro-surfacing mixture incorporating photocatalytic

additives can be used as functional materials for road exhaust purification.

The micro-surfacing mixture has a similar treatment cost as the chip seal, which is lower than the maintenance cost of most treatment strategies of hot mix asphalt mixtures. Micro-surfacing mixture has good economic benefits according to the comparison of highway maintenance technology cost data in California over the past 35 years [29]. However, in a Texas Transportation Institute report, the study pointed out that micro-surfacing mixture had the worst cracking resistance among six types of preventive maintenance technology for old pavement [30], which presents a challenge to the traditional design of micro-surfacing mixture material composition.

Fibers are applied in the micro-surfacing mixture to improve the cracking-resistance and durability as the reinforcement materials. For example, Wright et al. [31] found that the indirect tensile modulus and fatigue life of micro-surfacing mixture with 0.20 wt% glass fiber could be increased by 20% and 200% respectively. Hou et al. [32] studied a fiber reinforced micro-surfacing technique aimed to solve pavement performance problems, such as cracking and deformation. Luo et al. [33] also investigated the performance of micro-surfacing mixture by adding fibers, as well as recommending the dosage of fiber. She found that the optimal dosage of fiber is 0.10 wt%~0.20 wt% by the weight of asphalt mixture, according to the performance change and economic influence of micro-surfacing mixture. So, the addition of the fiber material in micro-surfacing mixture appears to have a significant effect on the improvement of the tensile strength and bending strength of the composite material.

In this work, photocatalytic modified micro-surfacing mixture (PMM) was designed, which was enhanced by polypropylene (PP) fiber and nano-TiO$_2$. The road performance of sixteen PMMs with the different contents of PP and nano-TiO$_2$ will be evaluated by wet-track abrasion test, wheel rutting deformation test and low-temperature splitting test. VE gas degradation capacity of PMMs was investigated under visible light and Ultraviolet (UV) light. Furthermore, the environmental performance of PMM was evaluated by the life cycle assessment (LCA) methodology based on the possible savings in energy consumption and greenhouse gas (GHG) emission during material production, transportation, and construction phases.

2. Materials and methods

2.1. Materials

Cationic Styrene Butadiene Rubber (SBR) modified emulsified asphalt binder prepared independently was selected as a binder in this study. For the emulsified asphalt binder, the matrix applied was the SK-90 asphalt binder. Meanwhile, SBR latex, emulsifier and stabilizer dosage were 3.5%, 2.0% and 0.3% in the SBR emulsified asphalt binder, respectively. And the technical indexes were illustrated in Table 1. The nano-TiO$_2$ was obtained from Shanghai Jianghu Industrial Company, and the Polypropylene (PP) fiber was produced by Changzhou Tianyi Engineering Fibers Co. Ltd. The basic properties of nano-TiO$_2$ and PP fibers were illustrated in Table 2 and Table 3. The technical indicators of nano-TiO$_2$ and PP fibers can meet the requirements of related specifications (GB/T 19591–2004 and JT/T 533–2020, respectively). In addition, an S-4800 cold field emission scanning electron microscope (SEM) was used to obtain the apparent morphology of the nano-TiO$_2$, and the results were as shown in Fig. 3. Pure nano-TiO$_2$ was mainly composed of a great many irregular spherical nanoparticles. The apparent morphology exhibited large and dense clusters formed by the agglomeration of fine particles. The coarse and fine aggregate was made of basalt, and the fine aggregate and filler were limestone. The selected aggregate and filler satisfied the recommended performance guidelines for micro-surfacing mixture (ISSA A143, 2010).

Table 4
Aggregate gradation micro-surfacing mixture.

Sieve size/mm	Passing percentage/wt.%			Composite gradation	Type III gradation of ISSA guideline	
	5 ~ 10 mm	3 ~ 5 mm	0 ~ 3 mm		Lower limit	Upper limits
9.50	100.0	100.0	100.0	100.0	100	100
4.75	7.8	93.7	99.7	80.4	70	90
2.36	0.3	8.3	89.4	59.4	45	70
1.18	0.3	4.0	55.5	36.7	25	50
0.60	0.3	2.8	37.3	24.7	19	34
0.30	0.3	2.4	24.8	16.5	12	25
0.15	0.3	2.0	16.8	11.3	7	18
0.075	0.2	1.2	8.2	5.6	5	15

Table 5
The combinations of different amounts of TiO$_2$ and PP fibers.

TiO$_2$ amount replacement of filler	PP fibers amount			
	0 wt% (F$_0$)	0.1 wt% (F$_{0.1}$)	0.2 wt% (F$_{0.2}$)	0.3 wt% (F$_{0.3}$)
0 wt% of filler (T$_0$)	(T$_0$, F$_0$)	(T$_0$ F$_{0.1}$)	(T$_0$ F$_{0.2}$)	(T$_0$ F$_{0.3}$)
40 wt% of filler (T$_{40}$)	(T$_{40}$ F$_0$)	(T$_{40}$ F$_{0.1}$)	(T$_{40}$ F$_{0.2}$)	(T$_{40}$ F$_{0.3}$)
60 wt% of filler (T$_{60}$)	(T$_{60}$ F$_0$)	(T$_{60}$ F$_{0.1}$)	(T$_{60}$ F$_{0.2}$)	(T$_{60}$ F$_{0.3}$)
80 wt% of filler (T$_{80}$)	(T$_{80}$ F$_0$)	(T$_{80}$ F$_{0.1}$)	(T$_{80}$ F$_{0.2}$)	(T$_{80}$ F$_{0.3}$)

2.2. Experimental and method

2.2.1. Composition design of PMM

a. Aggregate Gradation.

According to international slurry surfacing association (ISSA) A143 guideline [34], the aggregate gradation types for micro-surfacing mixture are identified as Type II and Type III. Type III gradation was chosen for the overlay of the highway. The gradation of the micro-surfacing mixture was shown in Table 4.

b. Fillers.

Herein, twelve different combinations of nano-TiO$_2$ and PP fibers were designed to study the optimal content of these two fillers. The symbols of each PMM are given in Table 5.

c. Determination of optimal content of modified emulsified asphalt binder and water.

The optimum mixing ratio of modified emulsified asphalt binder and water were determined according to the mixing time test and the cohesion torque test in JTG E 20-T0754 [35]. Specifically, samples of all filler combinations with different content of binder and water were used

to test the allowable mixing time under the same conditions of water-binder ratio (1:1.2) and cement content (2 wt%), which was determined by the previous mixing attempts. Because PP fibers can absorb modified emulsified asphalt binder, the content of modified emulsified asphalt binder increases with the increase of the amount of fiber, which is set as 6.8 wt%, 7.0 wt%, 7.2 wt% and 7.4 wt%, respectively. The results of mixing workability and cohesion are shown in Table 6. According to Table 6, with the increase of PP fibers content and binder content, the allowable mixing time was significantly extended at the same TiO$_2$ content level. Meanwhile, the rise in the proportion of TiO$_2$ led to an upward shift of allowable mixing time. 0.3% PP fibers exhibited a longer mixing time than others. It can be noted that the allowable mixing time and cohesion value of PMM with all the proportional compositions were satisfied with the specifications. It demonstrates the suitability of cement dosage and water-binder ratio. Furthermore, the ratios of each component of PMM were set as the preparation ratios for the test specimens in Table 6.

2.2.2. Road performance test

To investigate the wearability and stability of PMM, 800 g of the mixture was formed into a 280 mm diameter disc and the wet-track abrasion loss value of 1 h and 6d was measured according to JTG E 20-T0752.

The wheel rutting deformation test carried out at 25℃±2℃ was employed to measure rutting resistance of PMM. The specimen with a size of 380.0 mm × 50.0 mm × 12.7 mm was mounted on the bearing plate after drying. It was crushed 1000 times by the rubber wheel under a load of 56.7 kg and a rolling frequency of 44 times/min, then the width of the specimen after crushing was measured, and the wheel rutting deformation rate was calculated by the following formula:

$$PLD = (L_b - L_a) \times 100/L_a \qquad (1)$$

where, PLD represents the deformation rate of rut width, %; L_a and L_b are the widths of samples before and after rolling respectively, mm.

Considering that PMM is located at the upper layer of the pavement structure, which contacts directly with the atmospheric environment, so it is susceptible to temperature changes. Once the temperature suddenly drops, PMM is prone to low-temperature cracking. In this paper, the low-temperature splitting test was selected to evaluate the cracking resistance of PMM. The test specimen was a cylinder with a diameter of 101.6 mm and a height of 63.5 mm. The test temperature was set at −10℃±0.5℃, and the loading rate was 1 mm/min. Finally, the splitting tensile strength was used to characterize the low-temperature cracking resistance of PMM, which can be obtained by the equation (2):

Table 6
Results of mixture mixing time and cohesion torque test.

| TiO$_2$ amount replacement of filler (wt. %)	Fibers amount (wt. %)	Modified emulsified asphalt binder content (wt. %)	External water (wt. %)	Aggregate (wt. %)	Allowable mixing time (s)	Remarks	30 min Cohesion value (N·m)	60 min Cohesion value (N·m)
0	0.0	6.8	5.7	85.5	135	positive	1.2	2.0
	0.1	7.0	5.8	85.2	137	positive	1.3	2.1
	0.2	7.2	6.0	84.8	139	positive	1.4	2.1
	0.3	7.4	6.2	84.4	144	positive	1.3	2.0
40	0.0	6.8	5.7	85.5	136	positive	1.2	2.0
	0.1	7.0	5.8	85.2	137	positive	1.3	2.1
	0.2	7.2	6.0	84.8	140	positive	1.4	2.1
	0.3	7.4	6.2	84.4	143	positive	1.2	2.0
60	0.0	6.8	5.7	85.5	136	positive	1.2	2.0
	0.1	7.0	5.8	85.2	137	positive	1.2	2.2
	0.2	7.2	6.0	84.8	139	positive	1.4	2.3
	0.3	7.4	6.2	84.4	145	positive	1.3	2.2
80	0.0	6.8	5.7	85.5	138	positive	1.3	2.1
	0.1	7.0	5.8	85.2	140	positive	1.2	2.2
	0.2	7.2	6.0	84.8	144	positive	1.3	2.0
	0.3	7.4	6.2	84.4	148	positive	1.2	2.0
	Specification requirement						≥1.2	≥2.0
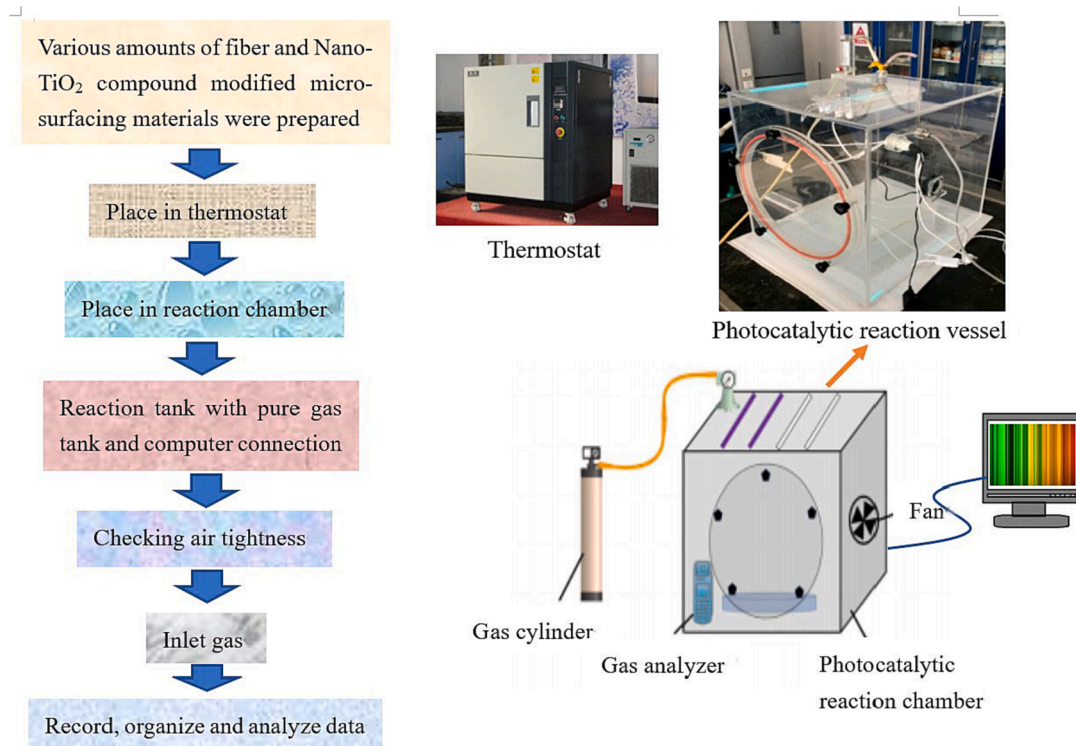
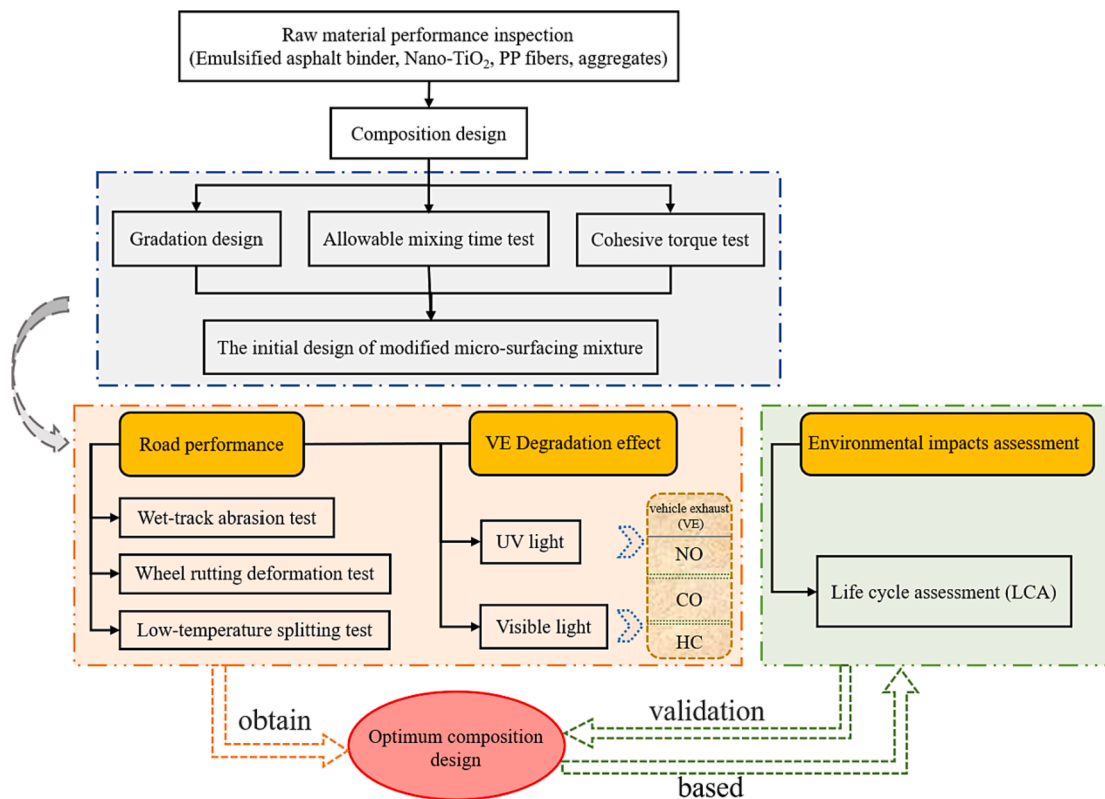**Fig. 4.** Photocatalytic degradation processes.

Fig. 5. The experimental flow diagram.

$$R_T = 0.006287 P_T / h \qquad (2)$$

where, R_T is the splitting strength, MPa; P_T is the maximum test load, N; and h is the height of the specimen, mm.

2.2.3. Photocatalytic degradation testing method

The photocatalytic degradation experiments were carried out by a self-made photocatalytic reaction vessel, and the specific operation process of the experiment and the digital photo of the VE removal

Table 7

Gas emissions inventory.

Type of Emission/consumption	Type of energy		
	Diesel	Heavy oil	Electricity
Energy Consumption	4.26E + 01	4.02E + 01	3.60E + 00
CO_2	6.71E-02	5.82E-02	1.24E-02
SO_2	8.65E-04	4.10E-04	3.11E-03
NO_x	5.95E-04	4.79E-04	2.30E-03
CO	1.75E-04	1.47E-04	1.39E-04
CH_4	1.44E-02	1.25E-02	2.25E-03
PM10	4.00E-06	3.45E-06	2.06E-06
NH_3	5.70E-06	4.90E-06	3.50E-06
C_2H_4	2.21E-07	1.92E-07	3.36E-09
CFC-11	1.45E-15	1.26E-15	2.65E-17
CFC-12	4.81E-20	4.18E-20	5.93E-21

reaction chamber were displayed in Fig. 4 [24,25]. The VE was specially prepared by Jining Xieli Special Gas Co., Ltd. The light source of the reaction chamber can be UV light (a wavelength in the range of 10–200 nm, the main wavelength was 38 nm) or visible light (a wavelength in the range of 400–700 nm, the main wavelength was 497 nm), and the light source was 50 cm away from the specimens. The air humidity in the reaction chamber was controlled at 40 ($\pm$3)%. The concentration of VE at a time was measured by A VE analyzer (NHA-506).

As shown in Fig. 4, VE reaction operation process was displayed. Briefly, PMM specimens with a diameter of 60 mm and a thickness of 10 mm were prepared and controlled humidity in the thermostat. And the sample shall be placed in an oven at 60℃ for more than 3 h to ensure curing before the photocatalytic degradation test. When the specimen fulfilled humidity and temperature, it was quickly placed in the vessel. The initial CO, NO and HC concentrations were controlled at 25 ppm $\pm$ 2 ppm. VE was transported into the vessel until the desired concentration was reached, and the fan was turned on to disperse the gas evenly. Lastly, UV or a visible light source in the vessel was turned on, and CO, NO and HC concentrations were recorded every 5 min for 90 min by NHA-506 VE analyzer. Since it was difficult to control the same initial concentration of VE, the degradation rate (η) was used as the index to compare and evaluate VE gas degradation capacity of PMM, which was calculated by Equation (3).

$$\eta = \frac{c_0 - c}{c_0} \times 100\% \tag{3}$$

where η is the degradation efficiency of CO, NO and HC, c_0 is the initial concentration of CO, NO and HC, c is the residual concentration after the reaction.

The framework of the test program in this paper was illustrated in
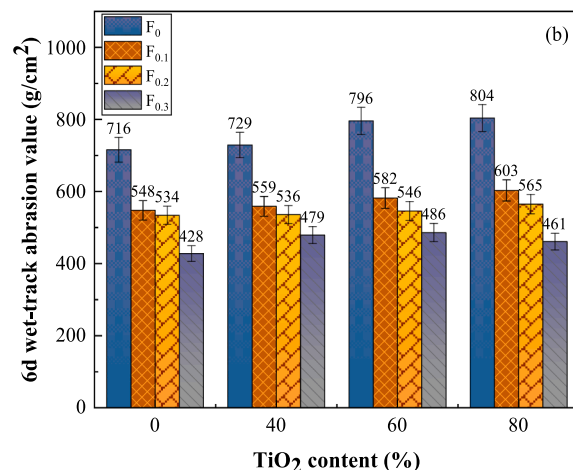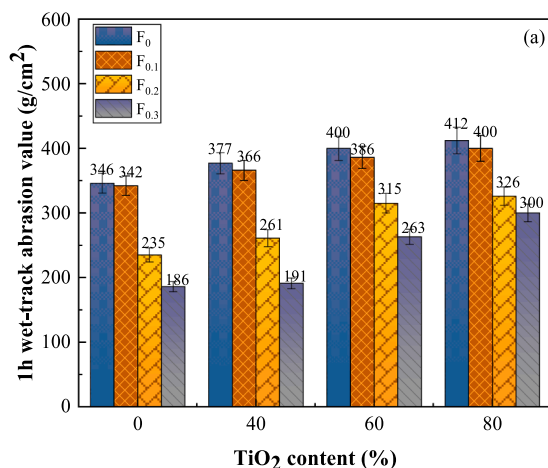
Fig. 5.

2.2.4. Environmental impacts method

The use of nano-TiO_2 as a photocatalytic additive in PMM can elicit the VE degradation effect. In addition to the environmental benefits of VE reduction, this PMM can bring potential energy savings and reduction in greenhouse gas (GHG) emissions by utilizing the PP fibers and nano-TiO_2.

In the conventional hot-mix asphalt mixture (HMA) production and paving stages, both the aggregate and the asphalt binder have to be heated to 160-180℃ to ensure that the aggregates are coated with asphalt binder in the asphalt mixing plant. Trucks transportation is needed for the conventional HMA from the asphalt mixing plant to the construction site. However, PMM can be produced and paved at the construction site at the environmental temperature. Meanwhile, PMM can be constructed without a paver, and only the roller compactor is necessary to compact the pavement smoothness. Therefore, PMM could save intensive energy compared with conventional HMA during the production, transportation, and construction process.

This study conducted a life cycle assessment (LCA) of PMM to evaluate its environmental impacts during the production, transportation,
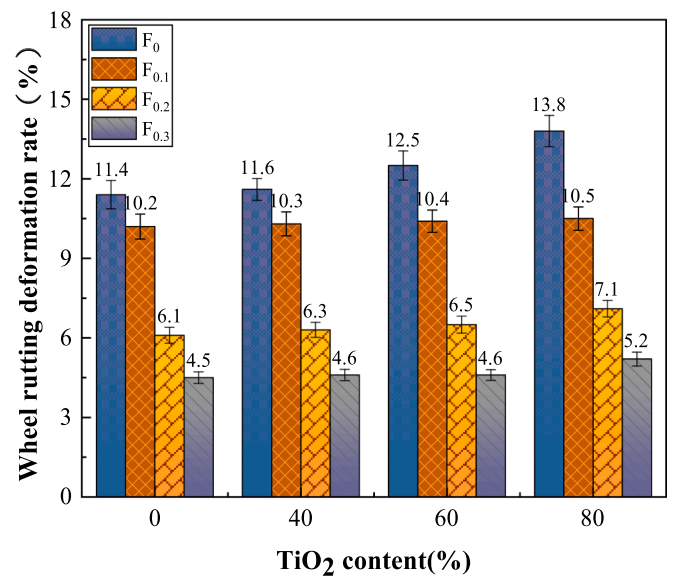

Fig. 7. Wheel rutting deformation rates with the different amounts of nano-TiO_2 and PP fibers.

Fig. 6. wet-track abrasion values with the different amounts of nano-TiO_2 and PP fibers: (a) 1 h, (b) 6 d.
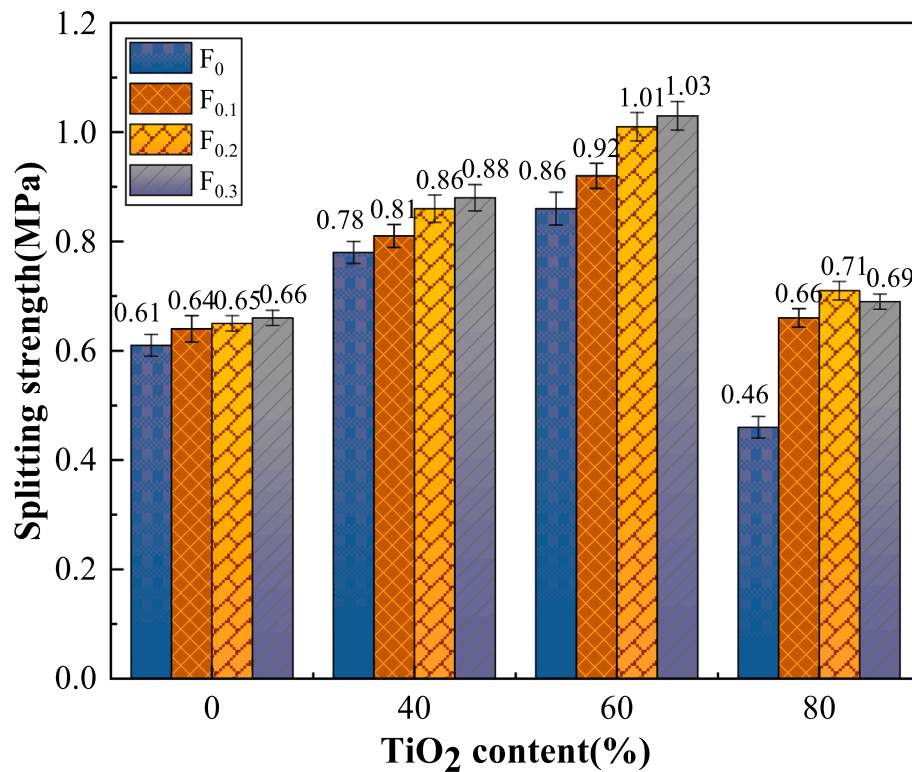
Fig. 8. Splitting strength results with different amounts of nano-TiO$_2$ and PP fibers.

and construction stages. This paper also compared the modified asphalt with two conventional asphalt mixtures, HMA and warm-mix asphalt mixture (WMA), to obtain more intuitive conclusions.

(1) Definition of objectives and scope.

One ton of PMM was selected as the functional unit. The boundary of the modified mixture is set from the start of asphalt mixture production until the asphalt mixture construction is completed, which includes the asphalt mixture production phase, transportation phase and construction phase stages.

(2) Inventory analysis.

PMM does not require heating in the production stage. A portable mixer with a capacity of 272 t/h was used according to the site visits, and thus an electricity consumption of 0.164 kWh was consumed. The energy consumption for HMA and WMA were calculated by the Green Asphalt Calculator. HMA consumes 0.125 kg diesel, 5.57 kg heavy oil and 3.43 kWh of electricity in this stage, while WMA consumes 0.096 kg diesel, 4.25 kg heavy oil and 2.62 kWh of electricity.

In the transportation stage, the mixed asphalt mixture is transported from the asphalt mixing plant to the construction site by a dump truck and poured into the paving machinery. During this phase, the environmental impact mainly comes from the fuel combustion of the transport vehicles. In this study, the average distance from the asphalt mixing plant to the construction site is assumed to be 30 km, the type of fuel is diesel, and the fuel usage rate is 0.23 kg/t*km. While the PMM can be produced at the pavement construction site, the transportation distance in the transportation phase is shorter than traditional asphalt material, which is approximately regarded as 10 km. PMM consumes 2.3 kg of diesel fuel, while the conventional HMA and WMA consume 6.9 kg of diesel fuel.

In the construction stage, energy consumption mainly originated from pavers and rollers. According to the data provided by the World Bank ROADEO software, the diesel consumption of asphalt paving machinery is 0.34 L/m^3 and that of rollers is 0.3 L/m^3. At this stage, the difference between PMM and the conventional HMA and WMA is that PMM only requires the use of rollers without pavers. Therefore, PMM

consumes 0.11 kg of diesel fuel, and HMA and WMA consume 0.234 kg of diesel fuel.

(3) Environmental impact evaluation.

The energy sources used throughout the life cycle of the three different types of asphalt mixtures are mainly diesel, heavy oil and electricity. The China life cycle database (CLCD) was queried to obtain a list of major gas emissions per unit of the three energy sources consumed, as shown in Table7. Energy use (EU), global warming potential (GWP), acidification potential (AP), ozone depletion potential (ODP), photochemical smog potential (POCP), and aerosol potential (AQP) are applied to evaluate the environmental impacts of three types of asphalt materials.

3. Results and discussions

3.1. Road performance

According to the wet-track abrasion test (WTAT), the wheel rutting deformation test and the low-temperature splitting test in JTG E 20 (T0752, T0756, T0716), respectively, the different PMM specimens were prepared. The results of the road performance tests are shown in Fig. 6, Fig. 7, Fig. 8.

3.1.1. Wet-track abrasion test results

The WTAT is applicable to evaluate the moisture damage resistance of PMM. Fig. 6 shows the results of the average wet-track abrasion values under soaking 1 h and 6d in a water bath at 25℃±1℃. It is obvious that the abrasion value of 1 h and 6 d decreased with the increase of PP fibers content, which indicate that PP fibers significantly improve the wear resistance of PMM. In addition, compared with F$_0$, the 6d wet-track abrasion values of F$_{0.1}$, F$_{0.2}$ and F$_{0.3}$ decrease significantly. However, for the results of 1 h wet-track abrasion test, F$_0$ and F$_{0.1}$ possess similar abrasion values, and the water damage resistance is more obvious when the content of PP fibers reaches above 0.2%. Because the soaking time is too short, it still has a complete structure that can resist
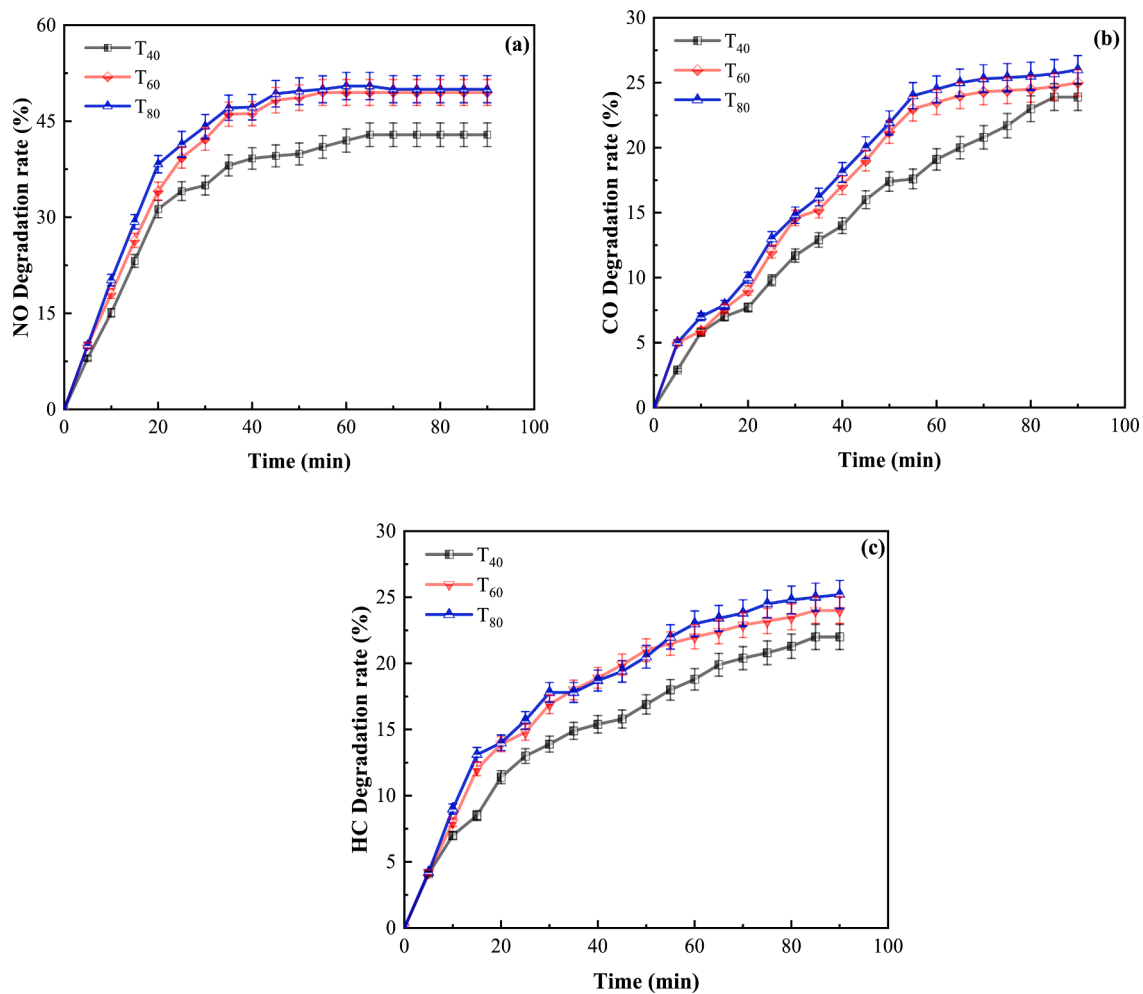
Fig. 9. The degradation effect under visible light: (a) NO, (b) CO, (c) HC.

water. The influence of 0.1 wt% PP fiber for the test results is not obvious.

On the other hand, the addition of nano-TiO$_2$ has a certain negative effect on the moisture damage resistance of PMM. This is mainly attributed to the fact that the density of TiO$_2$ is 4.26 g/cm^3, much higher than that of mineral powder (about 2.66 g/cm^3), which means that the substitution of TiO$_2$ for filler has a smaller volume and is difficult to fill the voids of aggregate. It greatly reduces the density of the mixture system, resulting in more vulnerability to water. Therefore, the lower content of nano-TiO$_2$ shows better moisture damage resistance. According to the above test results, the wet-track abrasion values of PMM with 0.3 wt% PP fibers and 0 wt% replacement of filler with nano-TiO$_2$ are the smallest in 1 h WTAT (186 g/m^2) and 6d WTAT (428 g/m^2), which proves that 0.3 wt% PP fibers are optimal.

3.1.2. Wheel rutting deformation test results

Fig. 7 shows that the addition of PP fibers led to a downward shifting of the wheel rutting deformation rates, indicating that the rutting resistance of PMM improves gradually. This result is in agreement with the previous research that the addition of fiber can absorb asphalt binder in a free state, and play the role of reinforcement, enhancing the strength and stability of the material [33], so it improves the rutting resistance of PMM. Moreover, it is worth remarking that as opposed to PP fibers, the addition of TiO$_2$ as a substitute of mineral powder resulted in the deterioration of rutting resistance of PMM. The main reason is that TiO$_2$ has no free charge on the surface, and it is difficult to interact with asphalt binder like mineral powder. Therefore, there is no chemical

adsorption effect on asphalt molecules, which greatly reduces the structural asphalt in PMM and increases the rutting disease.

3.1.3. Low-temperature splitting test results

It can be seen from Fig. 8 that it has a significant influence on the improvement of low temperature cracking of PMM with the amounts of PP fibers and nano-TiO$_2$ increase. When the amounts of nano-TiO$_2$ was 0 to 60 wt%, as the PP fibers increase from 0 to 0.3 wt%, the splitting strength of PMM increase by 0.1 wt%, which could be deduced that the bridging effect of PP fibers prevents the cracking of PMM [36,37]. On the other hand, splitting strength is increased with the amounts of nano-TiO$_2$ for the substitution rate range of 0 to 60 wt%, but the 80 wt% replacement of filler with nano-TiO$_2$ demonstrated a negative effect on the anti-cracking performance. When the content reached 80 wt%, the existence of a great many particles absorbed too much free asphalt binder in PMM due to the larger specific surface area of nano-TiO$_2$. Therefore, it reduced the cracking resistance of PMM, which indicated that the dosage of nano-TiO$_2$ should be strictly controlled.

3.2. Photocatalytic degradation effect

3.2.1. Study on the degradation effect under visible light conditions

The photocatalytic degradation effect of PMM under visible light is shown in Fig. 9. The degradation rates of T$_{60}$ and T$_{80}$ are significantly higher than those of T$_{40}$, while the variation trend with degradation time is roughly the same. Because the enhancement of photocatalytic active sites is caused by the increase of nano-TiO$_2$. The degradation efficiency
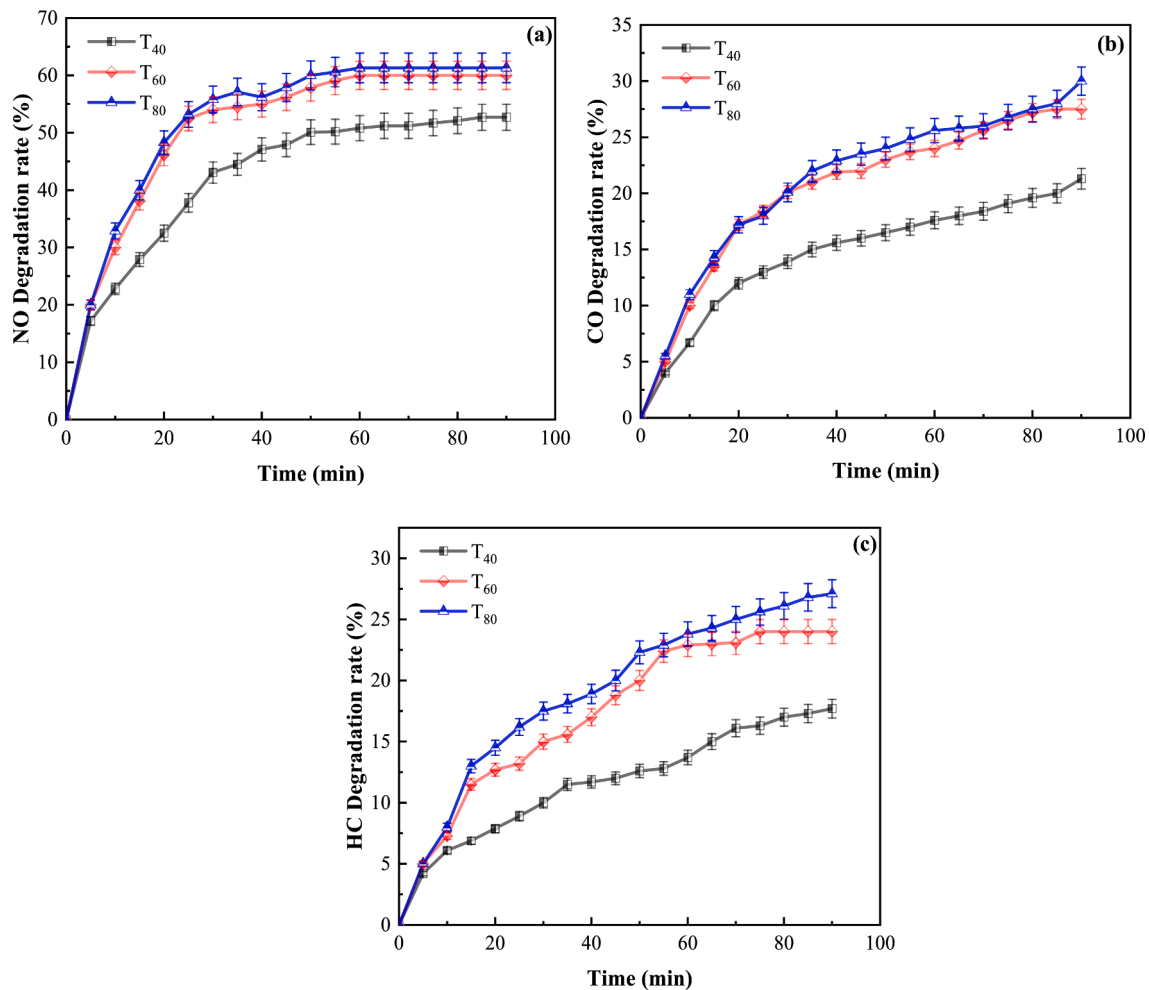
Fig. 10. The degradation effect under UV light: (a) NO, (b) CO, (c) HC.

of PMM is directly improved. In addition, it's worth noting that the degradation efficiency of PMM has no significant change, when the content of nano-TiO$_2$ exceeds 60 wt%. The main reason may be that the photocatalytic active sites have reached saturation due to the excess nano-TiO$_2$. At the same time, excessive photocatalytic materials agglomerate cannot play an effective role [25]. Hence, the recommended optimal dosage of nano-TiO$_2$ is 60 wt% by the weight of the mixture, balancing the photocatalytic degradation effect and economic influence of PMM.

Furthermore, the degradation rates of CO and HC are similar, but the degradation rate of NO is increased by 20% on average. It could be deduced that nano-TiO$_2$ has higher selectivity for NO. On the other hand, this result is highly beneficial for the degradation of VE based on NO accounts for a higher percentage of VE.

3.2.2. Study on the degradation effect under UV conditions

Fig. 10 presents the photocatalytic degradation efficiency of PMM with different amounts of nano-TiO$_2$ under ultraviolet irradiation. The degradation efficiency of the three gases under UV light has a high similarity with the trend of degradation efficiency under visible light. And there is a rapid reaction zone (generally for the first 20 min) and a stable zone during the process of photocatalytic reaction. Moreover, the degradation efficiency of CO and HC under UV light is slightly improved more than under visible light, while the highest degradation efficiency of NO reaches 60 %, which is 10% higher than that under visible light. This is mainly resulted from that the absorption intensity of nano-TiO$_2$ in the ultraviolet region is higher than that of visible light [25,38].

Furthermore, UV light has higher energy than visible light, which allows nano-TiO$_2$ to accelerate the rate of photocatalytic reactions more easily. Therefore, it could be deduced that PMM can degrade the harmful gas more effectively under UV light and the recommended optimal dosage of nano-TiO$_2$ is 60 wt% under both illumination conditions.

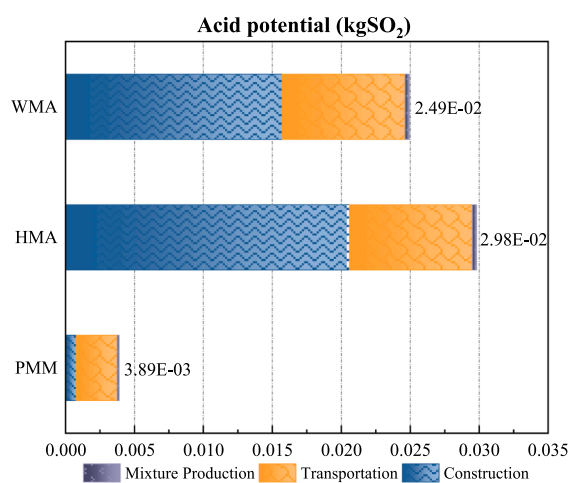### 3.3. Environmental impacts assessment

Six environmental impact indicators are chosen to evaluate the environmental impact of PMM and two conventional asphalt mixtures [39,40]. The environmental impact data associated with the respective life cycle stages is presented in Fig. 11. Results indicate that energy consumption of PMM markedly decreased, compared with HMA and WMA. The amount of energy consumption of PMM is four times more than HMA and WMA. Meanwhile, it can be noted that the GHG emission and other environmental impact indicators of PMM are lower than 20% of the HMA, and maintain at about 20% of the WMA, which proves that PMM is an environmentally friendly material. In addition, the data of the three mixtures in the whole life stage also show that the energy consumption and harmful gas emission of PMM mainly occur in the transportation stage, which can account for more than 95% of the whole life cycle. In summary, the environmental impact of PMM is less than that of the traditional HMA and WMA material in all stages, especially in the mix production stage, due to the characteristics of no need for heating and the possibility of in situ production. It indicates that PMM is a new type of environmentally friendly pavement material with certain competitiveness.
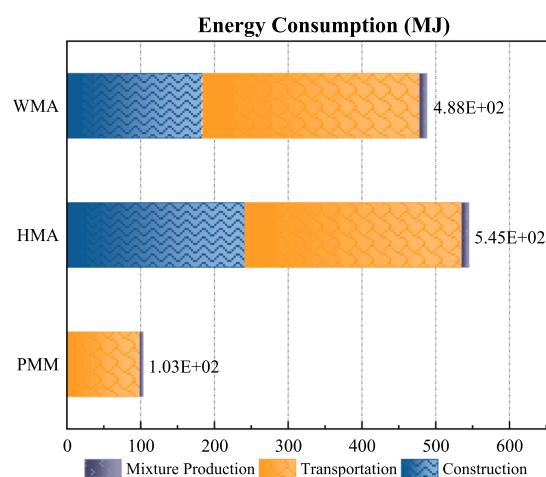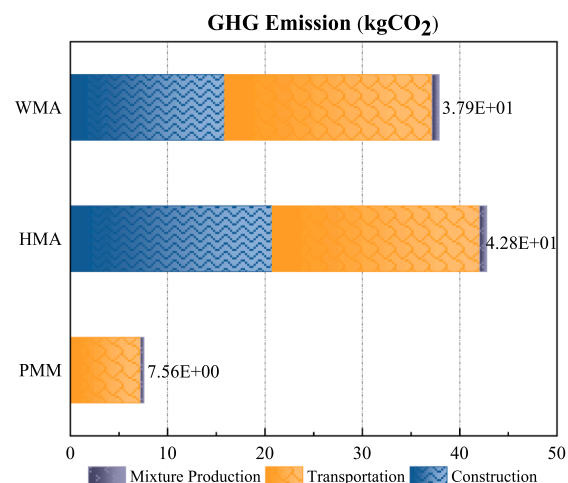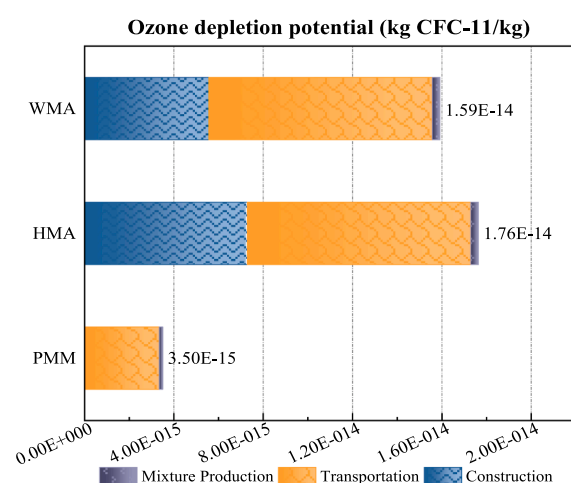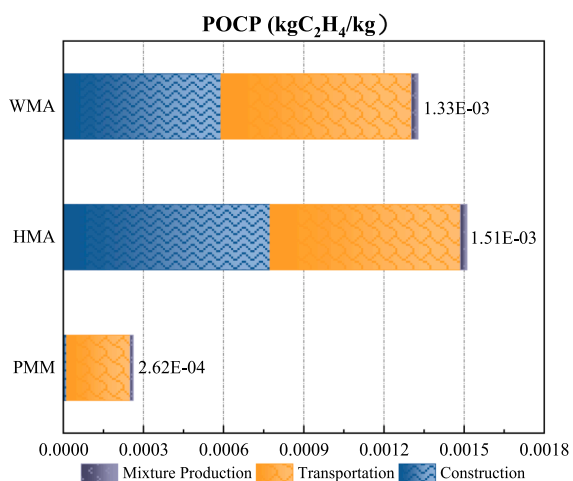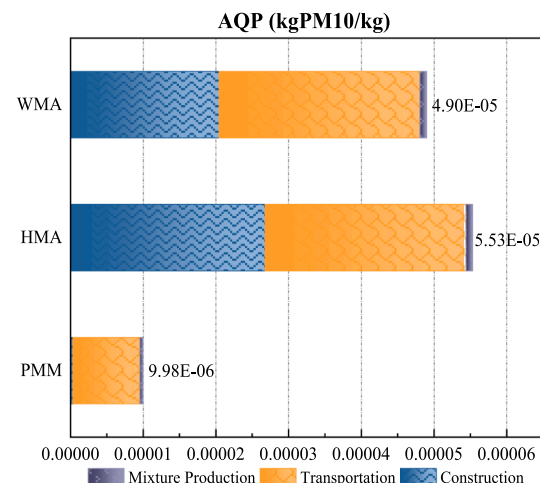
Fig. 11. Comparison of environmental impacts of PMM, HMA and WMA during production, transportation and construction.

4. Conclusions

In this work, an innovative type of PMM was designed, which was enhanced by PP fibers and nano-TiO_2. sixteen PMMs with the different contents of PP and nano-TiO_2 were prepared and utilized to evaluate road performances, VE gas degradation capacity and environmental impacts. Some conclusions can be drawn as follows:

(1). The addition of PP fibers improves the moisture damage resistance, the rutting resistance and low temperature cracking of PMM. The addition of nano-TiO_2 has a certain negative effect on the moisture damage resistance and the rutting resistance of PMM.

(2). NO, CO and HC degradation rates of PMM are significantly improved with the increase of nano-TiO_2, especially NO degradation rate. VE gas degradation capacity of PMM is better under UV light than that under visible light.

(3). PMM with 0.2 wt% PP fibers and 60 wt% replacement of mineral filler with nano-TiO_2 show excellent road performances and VE gas degradation capacity.

(4). Since PMM can be mixed, paved, and compacted in the field without the need for heating, it facilitates a significant reduction in energy consumption and greenhouse gas emissions.

In summary, the road performance, VE gas degradation capacity and environmental impacts of PMM were comprehensively investigated in the laboratory. In future work, the rheological properties of modified emulsified asphalt binder and its influence on the PMM will be explored. Meanwhile, trial road with PMM technique will be constructed and its road performance, VE gas degradation capacity and environmental impacts will be evaluated and studied.

CRediT authorship contribution statement

Zhao Zhang: Data curation, Writing – original draft. **Kai Liu:** Data curation, Writing – original draft. **Dan Chong:** Investigation, Writing – review & editing. **Dongyu Niu:** Supervision, Methodology, Writing – review & editing. **Peng Lin:** Supervision, Writing – review & editing. **Xueyan Liu:** Methodology, Writing – review & editing. **Yanhui Niu:** Investigation, Methodology. **Ruxin Jing:** Writing – review & editing.

Declaration of Competing Interest

The authors declare that they have no known competing financial interests or personal relationships that could have appeared to influence the work reported in this paper.

References

[1] J. Wang, Q. Wu, J. Liu, H. Yang, M. Yin, S. Chen, P. Guo, Vehicle emission and atmospheric pollution in China: problems, progress, and prospects, PeerJ 7 (2019), https://doi.org/10.7717/peerj.6932.

[2] Chinese Automotive Technology & Research Centre. (2017). Beijing Annals report on the development of China automotive industry 2015–2016. Chinese Automotive Technology & Research Centre Social Literature Science Press (in Chinese).

[3] M. Franklin, H. Vora, E. Avol, R. Mcconnell, F. Lurmann, F. Liu, B. Penfold, K. Berhane, F. Gilliland, W.J. Gauderman, Predictors of intra-community variation in air quality, J. Eposure Sci. Environ. Epidemiol. 22 (2) (2012) 135–147, https://doi.org/10.1038/jes.2011.45.

[4] X. Gao, T. Hu, K. Wang, Research on motor vehicle exhaust pollution monitoring technology, Appl. Mech. Mater. 620 (2014) 244–247, https://doi.org/10.4028/www.scientific.net/AMM.620.244.

[5] Ministry of Ecology and Environment of the People's Republic of China. (2017) Retrieved from: http://www.mee.gov.cn/gkml/sthjbgw/qt/201706/t20170603_415265.htm. (in Chinese).

[6] Y.-B. Zhao, P.-P. Gao, W.-D. Yang, H.-G. Ni, Vehicle exhaust: An overstated cause of haze in China, Sci. Total Environ. 612 (2018) 490–491.

[7] H. Tong, A.G. Rappold, M. Caughey, A.L. Hinderliter, D.W. Graff, J.H. Berntsen, W. E. Cascio, R.B. Devlin, J.M. Samet, Cardiovascular effects caused by increasing concentrations of diesel exhaust in middle-aged healthy GSTM1 null human volunteers, Inhalation Toxicol. 26 (6) (2014) 319–326, https://doi.org/10.3109/08958378.2014.889257.

[8] M. Foraster, A. Deltell, X. Basagaña, M. Medina-Ramón, I. Aguilera, L. Bouso, M. Grau, H.C. Phuleria, M. Rivera, R. Slama, J. Sunyer, J. Targa, N. Künzli, Local determinants of road traffic noise levels versus determinants of air pollution levels in a Mediterranean city, Environ. Res. J. 111 (1) (2011) 177–183.

[9] Z. Zheng, Z. Du, Q. Yan, Q. Xiang, G. Chen, The impact of rhythm-based visual reference system in long highway tunnels, Saf. Sci. 95 (2017) 75–82, https://doi.org/10.1016/j.ssci.2017.02.006.

[10] A. Albinet, I.J. Keyte, R.M. Harrison, On-road traffic emissions of polycyclic aromatic hydrocarbons and their oxy- and nitro-derivative compounds measured in road tunnel environments, Sci. Total Environ. 566 (2016) 1131–1142, https://doi.org/10.1016/j.scitotenv.2016.05.152.

[11] M. Chen, W. Liu, D. Lu, H. Chen, C. Ye, Progress of China's new-type urbanization construction since 2014: A preliminary assessment, Cities 78 (2018) (2014) 180–193, https://doi.org/10.1016/j.cities.2018.02.012.

[12] F. Yang, Y. Gao, K. Zhong, Y. Kang, Impacts of cross-ventilation on the air quality in street canyons with different building arrangements, Build. Sci. 104 (Aug.) (2016) 1–12, https://doi.org/10.1016/j.buildenv.2016.04.013.

[13] C. Guerreiro, V. Foltescu, F. Leeuw, Air quality status and trends in Europe, Atmos. Environ. 98 (Dec.) (2014) 376–384, https://doi.org/10.1016/j.atmosenv.2014.09.017.

[14] J.M. Nieuwenhuijsen, Urban and transport planning, environmental exposures and health-new concepts, methods and tools to improve health in cities, Environ. Health 15 (S1) (2016), https://doi.org/10.1186/s12940-016-0108-1.

[15] S. Squizzato, M. Cazzaro, E. Innocente, F. Visin, P.K. Hopke, G. Rampazzo, Urban air quality in a mid-size city — PM 2.5 composition, sources and identification of impact areas: From local to long range contributions, Atmos. Res. 186 (2016) 51–62, https://doi.org/10.1016/j.atmosres.2016.11.011.

[16] Z. Leng, H. Yu, Novel method of coating titanium dioxide on to asphalt mixture based on the breath figure process for air-purifying purpose, J. Mater. Civ. Eng. 28 (5) (2016).

[17] T. Wang, T. Xu, Photocatalytic activity of N-doped TiO_2 to vehicle exhaust in road tunnel, J. Test. Eval. 46 (3) (2018) 20170014, https://doi.org/10.1520/JTE20170014.

[18] C. Wang, Y. Li, X. Sun, Z. Gao, Automobile exhaust-purifying performance of tourmaline-modified asphalt concrete, J. Mater. Civ. Eng. 29 (6) (2017) 04017004, https://doi.org/10.1061/(ASCE)MT.1943-5533.0001818.

[19] W. Liu, S. Wang, J. Zhang, J. Fan, Photocatalytic degradation of vehicle exhausts on asphalt pavement by TiO_2/rubber composite structure, Constr. Build. Mater. 81 (apr.15) (2015) 224–232, https://doi.org/10.1016/j.conbuildmat.2015.02.034.

[20] V. Snapkauskiene, V. Valincius, V. Grigaitiene, Preparation and characterization of TiO_2-based plasma-sprayed coatings for NOx abatement, Catal. Today 191 (1) (2012) 154–158, https://doi.org/10.1016/j.cattod.2012.05.013.

[21] A. Fujishima, K. Hashimoto, T. Watanabe, TiO_2 photocatalysis: Fundamentals and applications, Russ. J. Electrochem. 35 (1999) 1137–1138.

[22] Y. Tan, L. Luo-Ke, P. Wei, Z. Sun, Application performance evaluation on material of automobile exhaust degradation in asphalt Pavement, Zhongguo Gonglu Xuebao/China J. Highway Transport 23 (6) (2010) 21–27.

[23] E. Boonen, A. Beeldens, Photocatalytic roads: from lab tests to real scale applications, Eur. Transp. Res. Rev. 5 (2) (2013) 79–89, https://doi.org/10.1007/s12544-012-0085-6.

[24] H. Xia, G. Liu, R. Zhang, L. Song, H. Chen, The photocatalytic degradation of vehicle exhausts by an Fe/N/Co–TiO_2 waterborne coating under visible light, Materials 12 (20) (2019), https://doi.org/10.3390/ma12203378.

[25] G. Liu, H. Xia, Y. Niu, X. Zhao, G. Zhang, L. Song, H. Chen, Photocatalytic performance of doped TiO_2/AC coating and its UV stability research, ScienceDirect Prog. Org. Coat. 148 (2020), 105882, https://doi.org/10.1016/j.porgcoat.2020.105882.

[26] F. Liu, M. Zheng, X. Fan, H. Li, F. Wang, Performance evaluation of waterborne epoxy resin-SBR compound modified emulsified asphalt micro-surfacing, Constr. Build. Mater. 295 (2021) 123588.

[27] S. Han, T. Yao, X. Han, Z. Hongwei, X. Yang, Performance evaluation of waterborne epoxy resin modified hydrophobic emulsified asphalt micro-surfacing mixture, Constr. Build. Mater. 249 (2020) 118835.

[28] P. Xu, J. Gao, J. Pei, R. Li, Z. Chen, Evaluation of NO_2-degradation by the rubber-titanium-aluminum ultrafine grained micro-surfacing material and its effect on pavement performance, Int. J. Pavement Res. Tech. 12 (1) (2019) 70–77, https://doi.org/10.1007/s42947-019-0009-0.

[29] Z. Wang, H. Zhou, V. Mandapaka, N. Lan, Pavement maintenance and rehabilitation practices in California: A study of 35-year as-built data in PaveM, Int. J. Trans. Sci. Tech. 10 (4) (2021) 380–392, https://doi.org/10.1016/j.ijtst.2021.04.005.

[30] T. Freeman, H. Ren, C. Spiegelman, D. Pinchott, Analysis and Treatment Recommendations form the Supplemental Maintenance Effectiveness Research Program (SMERP), Chip Seals, 2003.

[31] H. J. Wright, A. Choudhary, H. Akhlaghi, P. Price, (2013, September). Microsurfacing suspended fibre technology: product innovation: laboratory research investigation, Australia, 15th AAPA International Flexible Pavements Conference, 2013.

[32] S. Hou, H. Qiang, Experimental study on performances of fibre reinforced micro-surfacing mixture, J. Nanjing Univ. Technol. (Natural Science Edition) 3 (2013) 20–24.

[33] Y. Luo, K. Zhang, X. Xie, X. Yao, Performance evaluation and material optimization of Micro-surfacing based on cracking and rutting resistance, Constr. Build. Mater. 206 (2019) 193–200, https://doi.org/10.1016/j.conbuildmat.2019.02.066.

[34] International Slurry Surfacing Association. Recommended Performance Guidelines for Microsurfacing, ISSA A-143. ISSA, Glen Ellyn, Ill, 2010.

[35] JTG E20-2011 Standard test methods of bitumen and bituminous mixtures for highway engineering, Ministry of Communication, China, 2011.

[36] M.J. Kim, S. Kim, D.Y. Yoo, H.O. Shin, Enhancing mechanical properties of asphalt concrete using synthetic fibers, Constr. Build. Mater. 178 (2018) 233–243, https://doi.org/10.1016/j.conbuildmat.2018.05.070.

[37] S. Wang, R.B. Mallick, N. Rahbar, Toughening mechanisms in polypropylene fiber-reinforced asphalt mastic at low temperature, Constr. Build. Mater. 248 (2020), 118690, https://doi.org/10.1016/j.conbuildmat.2020.118690.

[38] J. Jin, T. Xiao, Y. Tan, J. Zheng, R. Liu, G. Qian, H. Wei, J. Zhang, Effects of TiO_2 pillared montmorillonite nanocomposites on the properties of asphalt with exhaust catalytic capacity, J. Clean. Prod. 205 (2018) 339–349, https://doi.org/10.1016/j.jclepro.2018.08.251.

[39] V.J. Ferreira, A. Sáez-De-Guinoa Vilaplana, T. García-Armingol, A. Aranda-Usón, C. Lausín-González, A.M. López-Sabirón, G. Ferreira, Evaluation of the steel slag incorporation as coarse aggregate for road construction: technical requirements and environmental impact assessment, J. Clean. Prod. 130 (2016) 175–186, https://doi.org/10.1016/j.jclepro.2015.08.094.

[40] H. Ma, Z. Zhang, X. Zhao, S. Wu, A comparative life cycle assessment (LCA) of warm mix asphalt (WMA) and hot mix asphalt (HMA) pavement: A case study in China, Adv. Civ. Eng. (2019) 1–12, https://doi.org/10.1155/2019/9391857.